of traveling waves expressed as (1), are omitted in the mode representation.

The resonance frequency for each eigen-excitation is never different from that for a standing wave in the x–y plane, since only the linear superimposition of the standing wave is made to obtain the traveling waves. The resonance frequency was determined for the idealized boundary conditions at the end of the ferrite post [2]. The lowest operation mode is given by $l = 1$, $m = -1$, and $n = 0$.

The resonance frequency split for the rotational phase eigen-excitations is related to the circulator bandwidth and the circulation direction. Resonance frequency variation due to permeability variation is given as follows [5]:

$$\frac{\Delta\omega^{\pm}}{\omega} = -\frac{\int (H^{\pm *} \cdot \Delta\tilde{\mu} H^{\pm})\, d\tau}{2\int \mu_0 |H^{\pm}|^2\, d\tau} \tag{19}$$

where μ_0 is the permeability when the ferrite is demagnetized, $\Delta\tilde{\mu} = \tilde{\mu} - \mu_0$, $H^{\pm}$ denotes magnetic field for rotational phase eigen-excitations, and $d\tau$ denotes the volume integral element.

When anisotropy is weak, $\Delta\tilde{\mu}$ may be approximated as follows:

$$\Delta\tilde{\mu} \fallingdotseq \begin{pmatrix} 0 & -j\kappa & 0 \\ j\kappa & 0 & 0 \\ 0 & 0 & 0 \end{pmatrix}. \tag{20}$$

Using (19) and (20),

$$\frac{\Delta\omega^{\pm}}{\omega} \fallingdotseq \frac{\kappa}{\mu} \frac{\int \mathrm{Im}(Hx^{\pm} Hy^{\pm *})\, d\tau}{\int |H^{\pm}|^2\, d\tau}$$

$$= \frac{\kappa}{\mu} \frac{\int \{\mathrm{Im}(Hx^{\pm})\mathrm{Re}(Hy^{\pm}) - \mathrm{Re}(Hx^{\pm})\mathrm{Im}(Hy^{\pm})\}\, d\tau}{\int |H^{\pm}|^2\, d\tau}. \tag{21}$$

When the ferrite post is completely short or open circuited at the two ends, the integrals along the ferrite axis in the numerator and the denominator are the same. Therefore, the volume integrations can be replaced by surface integration. In this case, the resonance frequency split is independent of the field variation along the ferrite post axis.

In the present approximation, the resonance frequency splits for the two rotational phase eigen-excitations are equal and opposite, as seen from (17) and (21).

For the lowest operation modes,

$$\frac{\Delta\omega^{\pm}}{\omega} = \pm \frac{\sqrt{3}}{2} \frac{\kappa}{\mu}. \tag{22}$$

The preceding result indicates a bandwidth of about two times compared with that of a cylindrical ferrite post lowest mode. Circulation directions are the same as those of the lowest cylindrical mode.

Acknowledgment

The author wishes to thank Y. Matsuo, A. Tomozawa, Y. Katoh, and Dr. H. Kaneko for their encouragement and guidance during the course of this work.

References

[1] B. Owen, "The identification of modal resonances in ferrite loaded waveguide Y-junctions and their adjustment for circulation," *Bell System Tech. J.*, vol. 51, pp. 595–627, Mar. 1972.
[2] Y. Akaiwa, "Operation modes of a waveguide Y circulator," *IEEE Trans. Microwave Theory Tech.* (Short Papers), vol. MTT-22, pp. 954–960, Nov. 1974.
[3] J. Helszajn and F. C. Tan, "Design data for radial-waveguide circulators using partial-height ferrite resonators," *IEEE Trans. Microwave Theory Tech.*, vol. MTT-23, pp. 288–298, Mar. 1975.
[4] N. Ogasawara and T. Noguchi, "Modal analysis of the dielectric slab of the normal triangular cross section," *Papers of the Technical Group of Microwave*, IECE Japan, June 1974 (in Japanese).
[5] R. F. Harrington, "*Time-Harmonic Electromagnetic Field*," New York: McGraw-Hill, 1961.

Electromagnetic Fields Induced Inside Arbitrary Cylinders of Biological Tissue

TE-KAO WU, MEMBER, IEEE, AND
LEONARD L. TSAI, MEMBER, IEEE

***Abstract*—The electromagnetic field induced inside arbitrary cross-sectioned cylinders of biological tissue is analyzed by integral equation and moment method techniques. A TM or TE plane wave incidence is assumed, and the cylinders consist of bone or muscle and may be multi-layered. The integral equations are of the *surface* type, and are derived via vector Green's theorem and boundary conditions. Surface and interior fields for both a one-layer and two-layer circular cylinder are found to have excellent agreements with the exact eigenfunction expansion results, thus validating the numerical method. Extensive results are presented for arbitrary cross-section cylinders, with among these an arm model composed of an elliptical outer muscle layer and a circular bone at the center. The field plots throughout the cylinder interior thus obtained should be useful in diagnostics of microwave hazards, particularly in predictions of the so-called "hot spots."**

I. Introduction

Biological effects of microwave radiation is an area of current concern [1]. The mechanisms by which electromagnetic fields penetrate biological tissues, and the potential hazards they pose, are just beginning to be investigated. Analytical predictions in the area have so far been rather limited. Primarily, treatments have been confined to structures which conform to a separable coordinate system (e.g., spheres or circular cylinders) [2]–[4]. For more realistic models with varied and arbitrary contours, the versatility of numerical techniques, i.e., moment method solution of integral equations, which have been extensively employed in other electromagnetic problems, should prove to be particularly advantageous.

In this short paper, coupled surface integral equations (SIE's) are first derived via Maxwell's equations, Green's theorem, and boundary conditions. The geometry of the analytical model to be treated consists of arbitrarily contoured cylinders (infinitely long in the z direction) of biological tissue illuminated by a TM or TE plane wave. The method is similar to that used by Tong [5], but differs significantly from the work of Livesay and Chen [6]. The solution of the integral equations for the surface fields then employs flat pulse expansion and point matching. Once the surface fields are found, fields everywhere interior to the cylinder are then readily determined.

To test the validity of this method, homogeneous circular cylinders of muscle and fatty tissue are first studied. The surface fields thus computed by integral equation methods are compared with the exact eigenfunction expansion results. Surface fields on homogeneous elliptical cylinders are next obtained to illustrate the arbitrary geometry capabilities of the integral equation solution. For a more complex structure, i.e., a two-layered composite cylinder of circular cross section, the surface fields obtained by the numerical solution are also compared with the exact solution. The extension in this next case is for an arm model

Manuscript received April 14, 1975; revised June 28, 1976.
The authors are with the Department of Electrical Engineering, University of Mississippi, University, MS 38677.

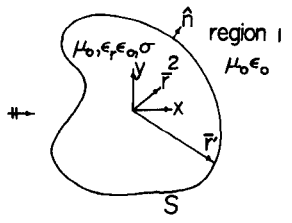

Fig. 1. Cross section of a homogeneous dielectric cylinder.

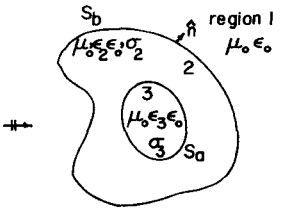

Fig. 2. Cross section of a two-layered composite dielectric cylinder.

consisting of an elliptical muscle layer with a circular bone in the center. Field plots throughout the interior for the preceding models are also obtained, and they hopefully may aid in diagnostics of hazards from so-called "hot spots."

II. Integral Equation Formulation

Consider a homogeneous lossy dielectric cylinder (infinitely long in the z direction, with μ_0, $\varepsilon_r\varepsilon_0$, and σ as permeability, permittivity, and conductivity, respectively) as depicted in Fig. 1. If the cylinder is illuminated by a TM incident plane wave, two coupled electric field integral equations may be derived from Maxwell's equations, Green's theorem, and the boundary conditions [5], [7], [8], [15], [16].

$$E_z^i(\bar{r}) = \frac{E_z(\bar{r})}{2} + \oint_S \left[G_1(\bar{r},\bar{r}') \frac{\partial E_z(\bar{r}')}{\partial n'} - E_z(\bar{r}') \frac{\partial G_1(\bar{r},\bar{r}')}{\partial n'} \right] dl' \quad (1)$$

and

$$0 = \frac{E_z(\bar{r})}{2} - \oint_S \left[G_2(\bar{r},\bar{r}') \frac{\partial E_z(\bar{r}')}{\partial n'} - E_z(\bar{r}') \frac{\partial G_2(\bar{r},\bar{r}')}{\partial n'} \right] dl' \quad (2)$$

where $\bar{r}$ and $\bar{r}'$ are radial vectors from the origin to the field and source points on the cylinder cross-sectional contour S. $\oint$ denotes the Cauchy principle value integral with singularities removed; its numerical treatment can be found in [16], [17]. $E_z(\bar{r})$ and $\partial E_z(\bar{r})/\partial n'$ are the unknown surface electric field and its normal derivatives, $E_z^i(\bar{r}) = e^{-jk_0x}$ is the incident electric field, $k_0 = \omega\sqrt{\mu_0\varepsilon_0}$ with a $e^{j\omega t}$ time dependence, and $\hat{n}$ is the unit outward normal to S. The two-dimensional Green's function is given by

$$G_i(\bar{r},\bar{r}') = -\frac{j}{4} H_0^{(2)}(k_i|\bar{r} - \bar{r}'|) \quad (3)$$

where $H_0^{(2)}$ is the second kind and zeroth-order Hankel function; its numerical evaluation follows standard procedures in [13], [14], $i = 1$ or 2, with 1 denoting the exterior to the cylinder and 2 denoting the cylinder interior, $k_1 = k_0$, and

$$k_2 = k_0\sqrt{\varepsilon_r - j\sigma/(\omega\varepsilon_0)}.$$

The solution for the surface fields $E_z(\bar{r})$ and $\partial E_z(\bar{r})/\partial n$ from the coupled integral equations (1) and (2) may now be readily obtained by the method of moments [9]. Specifically, the contour S is first divided into M segments each of width ΔS_n, then $E_z(\bar{r})$ and $\partial E_z(\bar{r})/\partial n$ are expanded in sets of flat pulse basis functions, i.e.,

$$E_z(\bar{r}) = \sum_{n=1}^{M} A_n P_n(\bar{r})$$
$$\frac{\partial E_z(\bar{r})}{\partial n} = \sum_{n=1}^{M} B_n P_n(\bar{r}) \quad (4)$$

where A_n and B_n are the unknown coefficients to be found, $P_n(\bar{r}) = 1$ for $\bar{r} \in \Delta S_n$, and $P_n(\bar{r}) = 0$ otherwise. Substituting (4) into (1) and (2), and requiring (1) and (2) to hold only at the midpoint of each segment (i.e., point matching) results in a matrix equation for determining the unknown coefficients. Once the unknown coefficients A_n and B_n are found, fields everywhere interior to the cylinder are calculated from

$$E_z(\bar{r}) = \int_S \left[G_2(\bar{r},\bar{r}') \frac{\partial E_z(\bar{r}')}{\partial n'} - E_z(\bar{r}') \frac{\partial G_2(\bar{r},\bar{r}')}{\partial n'} \right] dl' \quad (5)$$

where $\bar{r}$ is in region 2 and $\bar{r}'$ is on S.

If the cylinder is illuminated by a TE incident plane wave, two coupled magnetic field integral equations are derived using the same reasoning as for (1) and (2).

$$\frac{H_z(\bar{r})}{2} = H_z^i(\bar{r}) + \oint_S \left[H_z(\bar{r}') \frac{\partial G_1(\bar{r},\bar{r}')}{\partial n'} - \frac{\varepsilon_0}{\hat{\varepsilon}} G_1(\bar{r},\bar{r}') \frac{\partial H_z(\bar{r}')}{\partial n'} \right] dl' \quad (6)$$

and

$$\frac{H_z(\bar{r})}{2} = -\oint_S \left[H_z(\bar{r}') \frac{\partial G_2(\bar{r},\bar{r}')}{\partial n'} - G_2(\bar{r},\bar{r}') \frac{\partial H_z(\bar{r}')}{\partial n'} \right] dl' \quad (7)$$

where $\bar{r}$ and $\bar{r}'$ are on S, $\hat{\varepsilon} = \varepsilon_r\varepsilon_0 - j\sigma/\omega$, $H_z^i(\bar{r}) = e^{-jk_0x}$ is the incident magnetic field, and $H_z(\bar{r})$ and $\partial H_z(\bar{r})/\partial n$ are the unknown surface field and its normal derivatives which may now be readily obtained by the same solution procedure as described in the TM case. Once the surface fields are found the interior field is calculated from

$$H_z(\bar{r}) = \int_S \left[G_2(\bar{r},\bar{r}') \frac{\partial H_z(\bar{r}')}{\partial n'} - H_z(\bar{r}') \frac{\partial G_2(\bar{r},\bar{r}')}{\partial n'} \right] dl' \quad (8)$$

where $\bar{r}$ is in region 2 and $\bar{r}'$ is on S.

Consider now a two-layered composite lossy dielectric cylinder as depicted in Fig. 2. If a TM incident plane wave is assumed, four coupled electric field integral equations are obtained again using the same reasoning as in (1) and (2).

$$0 = \frac{E_{za}(\bar{r})}{2} + \oint_{S_a} \left[E_{za}(\bar{r}') \frac{\partial G_3(\bar{r},\bar{r}')}{\partial n'} - G_3(\bar{r},\bar{r}') \frac{\partial E_{za}(\bar{r}')}{\partial n'} \right] dS', \quad \text{for } \bar{r} \in S_a \quad (9)$$

$$0 = \frac{E_{za}(\bar{r})}{2} + \int_{S_b} \left[E_{zb}(\bar{r}') \frac{\partial G_2(\bar{r},\bar{r}')}{\partial n'} - G_2(\bar{r},\bar{r}') \frac{\partial E_{zb}(\bar{r}')}{\partial n'} \right] d\,' - \oint_{S_a} \left[E_{za}(\bar{r}') \frac{\partial G_2(\bar{r},\bar{r}')}{\partial n'} - G_2(\bar{r},\bar{r}') \frac{\partial E_{za}(\bar{r}')}{\partial n'} \right] dS', \quad \text{for } \bar{r} \in S_a \quad (10)$$

$$0 = \frac{E_{zb}(\bar{r})}{2} + \oint_{S_b} \left[E_{zb}(\bar{r}') \frac{\partial G_2(\bar{r},\bar{r}')}{\partial n'} - G_2(\bar{r},\bar{r}') \frac{\partial E_{zb}(\bar{r}')}{\partial n'} \right] dS' - \int_{S_a} \left[E_{za}(\bar{r}') \frac{\partial G_2(\bar{r},\bar{r}')}{\partial n'} - G_2(\bar{r},\bar{r}') \frac{\partial E_{za}(\bar{r}')}{\partial n'} \right] dS', \quad \text{for } \bar{r} \in S_b \quad (11)$$

and

$$E_z^{\text{inc}}(\bar{r}) = \frac{E_{zb}(\bar{r})}{2} - \int_{S_b} \left[E_{zb}(\bar{r}') \frac{\partial G_1(\bar{r},\bar{r}')}{\partial n'} - G_1(\bar{r},\bar{r}') \frac{\partial E_{zb}(\bar{r}')}{\partial n} \right] dS', \quad \text{for } \bar{r} \in S_b \quad (12)$$

where

$$E_{za}(\bar{r}) \quad \frac{\partial E_{za}(\bar{r})}{\partial n'} \quad E_{zb}(\bar{r}) \quad \frac{\partial E_{zb}(\bar{r})}{\partial n'}$$

are the unknown surface fields and their normal derivatives to be found.

$$E_z^{\text{inc}}(\bar{r}) = e^{-jk_1 x}$$

is the TM incident plane wave,

$$G_i(\bar{r},\bar{r}') = \frac{j}{4} H_0^{(2)}(k_i|\bar{r} - \bar{r}'|)$$

$$k_i = \omega\sqrt{\mu_0 \varepsilon_i \varepsilon_0}, \qquad i = 1,2,3$$

with $k_1 = k_0 = \omega\sqrt{\mu_0\varepsilon_0}$, where $\hat{n}$ is the unit outward normal to S_a or S_b.

Similar to the single-layered cylinder case, the unknown surface fields and normal derivatives are also obtained using flat pulse expansion and point matching. Once the surface fields are found, the fields interior to the cylinder may readily be obtained from

$$E_z(\bar{r}) = \int_{S_a} \left[G_3(\bar{r},\bar{r}') \frac{\partial E_{za}(\bar{r}')}{\partial n'} - E_{za}(\bar{r}') \frac{\partial G_3(\bar{r},\bar{r}')}{\partial n'} \right] dS', \quad \text{for } \bar{r} \in \text{region 3} \quad (13)$$

and

$$E_z(\bar{r}) = \int_{S_a} \left[E_{za}(\bar{r}') \frac{\partial G_2(\bar{r},\bar{r}')}{\partial n'} - G_2(\bar{r},\bar{r}') \frac{\partial E_{za}(\bar{r}')}{\partial n'} \right] dS' - \int_{S_b} \left[E_{zb}(\bar{r}') \frac{\partial G_2(\bar{r},\bar{r}')}{\partial n'} - G_2(\bar{r},\bar{r}') \frac{\partial E_{zb}(\bar{r}')}{\partial n'} \right] dS', \quad \text{for } \bar{r} \in \text{region 2.} \quad (14)$$

For a TE incident plane wave, four coupled magnetic field integral equations may also be straightforwardly derived. The details are given in [16].

For homogeneous or two-layered lossy dielectric *circular* cylinders, the eigenfunction expansion method provides the exact solution. Since this is a two-dimensional scattering problem, standard cylindrical harmonic functions [10] may be employed to represent the fields in each region. Applying boundary conditions (i.e., continuous tangential E and H fields at the interface), a set of simultaneous equations are obtained for finding the unknown coefficients in the field expansion series. Once the coefficients are obtained, fields everywhere interior to the cylinder may readily be calculated. The details can be found in [12], [16], [19].

III. Results and Discussion

Numerical results for the surface fields on circular cylinders of both muscle and fatty tissue are first computed using both the SIE technique and the eigenfunction expansion methods. Excellent agreement between the two methods is obtained [15], [16]; thus the numerical solution can be considered valid. Rapid convergence of the SIE solutions (with only ten pulses for each circular cross-sectional contour) is also observed [16]. Results obtained for lossy dielectric cylinders also seem to indicate that the number of samples required for convergence is about the same as for perfectly conducting cylinders [9], [16].

One of the main objectives of this study is to find means which may aid in the detection of resonance effects and possible hot spots. Toward that end, the fields throughout the interior of the previous models are examined. Computation of interior fields are performed using (5), (8), (13), and (14), from the now known surface fields, and with eight-point Gaussian quadrature integration [13] over each surface pulse. To provide a detailed graphical depiction of interior variations, contour plots of the field magnitudes for the various models are given in Figs. 3–10. It should be noted that since the E-field plot is related to the time-average volumetric tissue-absorbed power density (i.e., $p = \frac{1}{2}\sigma\bar{E} \cdot \bar{E}^*$ [20]), these field plots will be useful to biological researchers in microwave hazards assessment and the estimation of the total amount of power absorbed by the tissue body.

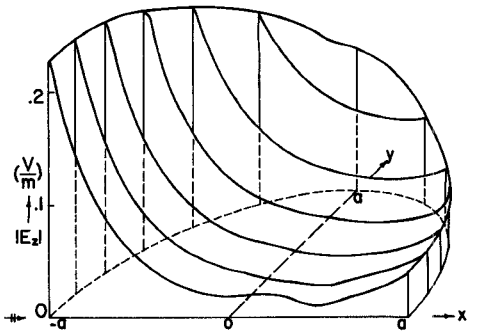

Fig. 3. E-field plot for a circular cylinder of muscle ($\varepsilon_r = 60$, $\sigma = 1$ ℧/m, $a = 0.159$ m, $f = 300$ MHz, TM incident wave).

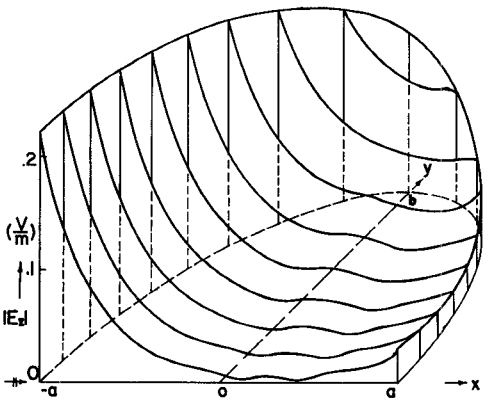

Fig. 4. E-field plot for an elliptical cylinder of muscle ($\varepsilon_r = 60$, $\sigma = 1$ ℧/m, $a = 0.159$ m, $b = 0.239$ m, $f = 300$ MHz, TM incident wave).

In Figs. 3 and 4, field contour plots for a one-layer circular and elliptical cylinder of muscle ($\varepsilon_r = 60$, $\sigma = 1$ ℧/m, $a = 6.25$ in, $b = 1.5a$) illuminated by a TM polarized plane wave (frequency = 300 MHz) are given. Notice that because of symmetry, it is necessary to show only the upper half of the cylinder. It may be observed that since muscle possesses a relatively high conductivity, the fields are rapidly attenuated from the front to the back of the cylinder. The same trend, however, does not apply for cylinders of fatty tissue or bone, whose contour plots are given in Figs. 5 and 6 (with $\varepsilon_r = 5$, $\sigma = 0.017$ ℧/m). Here, because resonance effects are not significantly attenuated, the interior fields oscillate strongly. In fact, not only are the field strengths at the back of the cylinder actually larger than at the front, but through large regions the interior field strength may be even higher than the incident illumination. Similar trends and behaviors have also been observed for the TE case [16].

Field contour plots for the two-layered cylinders are given in Figs. 7–10. Fig. 7 shows the trends for the circular cylinder, where a circular layer of muscle ($\varepsilon_2 = 49$, $\sigma_2 = 0.40425$ ℧/m, $b = 15$ cm) encases a circular bone ($\varepsilon_3 = 6.2$, $\sigma_3 = 0.08525$ ℧/m, $a = 10$ cm) at 300 MHz. Notice that because the muscle layer is relatively thin, the attenuation is weak and significant

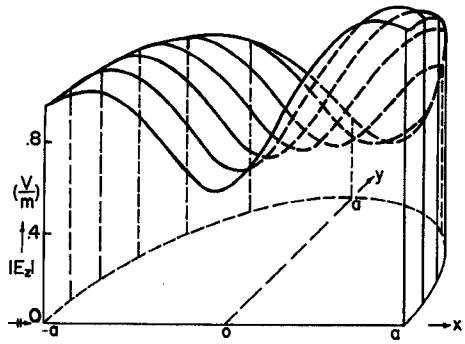

Fig. 5. E-field plot for a circular cylinder of bone or fat ($\varepsilon_r = 5$, $\sigma = 0.017$ ℧/m, $a = 0.159$ m, $f = 300$ MHz, TM incident wave).

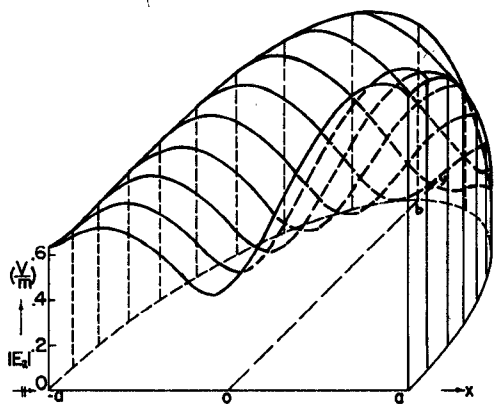

Fig. 6. E-field plot for an elliptical cylinder of bone or fat ($\varepsilon_r = 5$, $\sigma = 0.017$ ℧/m, $a = 0.159$ m, $b = 0.239$ m, $f = 300$ MHz, TM incident wave).

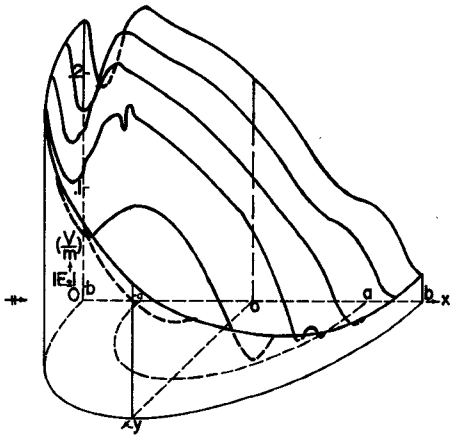

Fig. 7. E-field plot for a composite cylinder of circular muscle ($\varepsilon_2 = 49$, $\sigma = 0.404$ ℧/m, $b = 0.15$ m, $f = 300$ MHz) encasing circular bone ($\varepsilon_3 = 6.2$, $\sigma_3 = 0.085$ V/m, $a = 0.1$ m, TM incident wave).

resonance effects still remain in the central bone region. For the arm model consisting of an elliptical muscle layer ($\varepsilon_2 = 55$, $\sigma = 1.1$ ℧/m, $b = 9$ cm, $g = 6.5$ cm) encasing a circular bone ($\varepsilon_3 = 6$, $\sigma = 0.04$ ℧/m, $a = 2$ cm), the trends are given in Fig. 8. Here the comparatively quicker muscle layer significantly attenuates the wave, with the result that resonance effects in the central bone region, though still perceptible, now become somewhat inconsequential.

Figs. 9 and 10 show the H- and E-field plots for the same composite circular cylinder as in Fig. 7, now with a 300 MHz, TE incident plane wave. It should be remarked that in Fig. 10, for computational convenience, the exact solution rather than the integral equation is used. The trends in the H field are similar to those observed before (for the E field of the TM case). The E

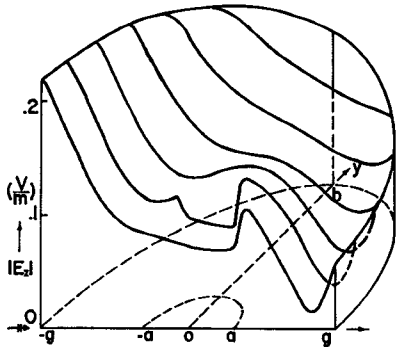

Fig. 8. E-field plot for a composite dielectric cylinder of elliptical muscle ($\varepsilon_2 = 55$, $\sigma_2 = 1.1$ ℧/m, g $= 6.5$ cm, $b = 9$ cm, $f = 300$ MHz) encasing circular bone ($\varepsilon_3 = 6$, $\sigma_3 = 0.04$ ℧/m, $a = 2$ cm, TM incident wave).

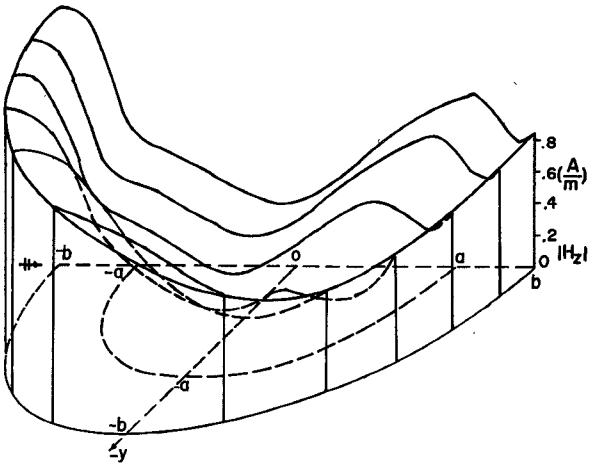

Fig. 9. H-field plot for the same cylinder as in Fig. 7, with TE excitation.

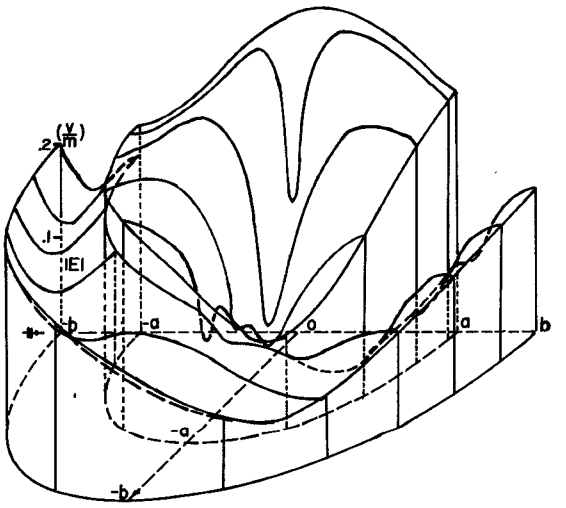

Fig. 10. E-field plot for the same cylinder as in Fig. 7, with TE excitation.

field in this case, however, exhibits drastically different behaviors. Not only does there exist a discontinuity at the interface, as it should, but also a null is now present. Notice that the null location is away from the cylinder axis, reminding one of field distributions in circular waveguides. Thus different resonance mechanisms are evidently occurring in the TE case as compared to the TM case.

It should be noted, in closing, that though only field magnitudes are shown, phase information is also available from this analysis. By proper correlation of these results with experimental thermo-

TABLE I
COMPARISON OF THE NUMBER OF UNKNOWNS BETWEEN SIE'S AND VIE'S

	SIE	VIE
Square cylinder with N samples on each side	8N	N^2
Cube with N samples on each side	$24N^2$	$3N^3$

graphic data, and by extrapolating bulk dosimetry trends through analysis of many models and parameters similar to the aforementioned one, it is believed that this analysis should constitute a useful diagnostic tool for predicting microwave hazards.

IV. Concluding Remarks

In this short paper the feasibility of using the SIE technique to analyze the fields in arbitrarily shaped lossy dielectric cylinders with a TM or TE incident plane wave has been demonstrated. Generally, this method also applies for any arbitrarily shaped penetrable cylinders composed of both dielectric and magnetic material. Although the illuminating sources considered here are TM and TE plane waves, for near zone sources such as direct contacted aperture sources, corner reflectors, etc., this technique still applies. For dielectric circular cylinders, good agreement is obtained between the SIE solutions and the eigenfunction expansion solutions. For a cylinder with arbitrary cross section, however, the integral equation method, including both the SIE method of this short paper and the volume integral equation (VIE) technique advocated in [6], [11], proves to be definitely more advantageous.

A further breakdown of the comparable computer storage requirement of the two integral equation methods is now in order, since this dictates the maximum sampling rate and hence body size which may be tractable. For conceptual simplicity consider the homogeneous square cylinder and cube. Table I shows the relative number of unknowns, and thus the matrix size, needed for each [16]. To assure that meaningful results are obtained, i.e., sufficient sampling to accurately describe field variations, N should be large. Thus the SIE can be seen to hold a definite advantage (for $N > 8$). It should also be noted that the same sampling rate is assumed for the VIE throughout the interior. In cases where ε_r or σ are large, and wavelength becomes contracted inside the body, a much larger number of samples than that assumed here may actually be needed. If the body is not homogeneous, however, i.e., many layered or even with continuously varying ε and σ, then the VIE approach should prove to be more suitable.

In order to aid in the determination of applicability, the major advantages of each method are summarized here.

VIE Technique:

1) Applicable for arbitrary geometric configurations.
2) Avoids convergence problem of the eigenfunction series.
3) Useful for inhomogeneous bodies.

SIE Technique:

1) Less unknowns are required for homogeneous bodies.
2) Applicable for arbitrary geometric configurations.
3) Avoids convergence problem of the eigenfunction series.

Eigenfunction Expansion Technique:

1) Does not require the storage and inversion of a large matrix.
2) Requires much less computer time.

In conclusion, the problem of predicting fields in arbitrary cylinders of biological tissue has been successfully treated. By the good agreement obtained and useful field contours found, one may conclude that the numerical techniques employed here are advantageous tools. This solution method has also been successfully applied to three-dimensional bodies of revolution [18] and will be presented in a later paper.

Acknowledgment

The authors wish to thank Dr. D. R. Wilton for his many suggestions during the course of this work.

References

[1] W. W. Mumford, "Introductory remarks," *IEEE Trans. Microwave Theory Tech. (Special Issue on Biological Effects of Microwaves)*, vol. MTT-19, p. 130, Feb. 1971.
[2] A. R. Shipiro, R. F. Lutomirski, and H. T. Yura, "Induced fields and heating within a cranial structure irradiated by an electromagnetic plane wave," *IEEE Trans. Microwave Theory Tech.*, vol. MTT-19, pp. 187–196, Feb. 1971.
[3] H. S. Ho, A. W. Guy, R. A. Sigelmann, and J. F. Lehmann, "Microwave heating of simulated human limbs by aperture sources," *IEEE Trans. Microwave Theory Tech.*, vol. MTT-19, pp. 224–231, Feb. 1971.
[4] A. W. Guy, "Analyses of electromagnetic fields induced in biological tissues by thermographic studies on equivalent phantom models," *IEEE Trans. Microwave Theory Tech.*, vol. MTT-19, pp. 205–214, Feb. 1971.
[5] T. C. Tong, "Scattering by a dielectric rectangular cylinder," presented at the 1973 IEEE G-AP Symposium, Boulder, CO, Aug. 1973.
[6] D. E. Livesay and K. M. Chen, "Electromagnetic fields induced inside arbitrarily shaped biological bodies," *IEEE Trans. Microwave Theory Tech.*, vol. MTT-22, pp. 1273–1280, Dec. 1974.
[7] J. A. Stratton, *Electromagnetic Theory*. New York: McGraw-Hill, ch. 3, 1941.
[8] A. J. Poggio and E. K. Miller, "Integral equation solutions of three-dimensional scattering problems," *Computer Techniques for Electromagnetics*, R. Mittra Ed., Pergamon Press, 1973.
[9] R. F. Harrington, *Field Computation by Moment Methods*. New York: McGraw-Hill, pp. 230–238, 261, 1961.
[10] R. F. Harrington, *Time Harmonic Electromagnetic Fields*. New York: McGraw-Hill, 1961.
[11] J. H. Richmond, "Scattering by a dielectric cylinder of arbitrary cross section shape," *IEEE Trans. Antennas Propagat.*, vol. AP-13, p. 334, May 1965.
[12] T. K. Wu and L. L. Tsai, "Shielding properties of thick conducting cylindrical shells," *IEEE Trans. Electromag. Compat.*, vol. EMC-16, pp. 201–204. Nov. 1974.
[13] M. Abramowitz and T. Stegun, *Handbook of Mathematical Functions*, NBS AMS-55.
[14] J. E. Lewis, T. K. Sarkar, and P. D. O'Kelly, "Generation of Bessel functions of complex order and argument," *Electron. Lett.*, vol. 7, pp. 615–616, Oct. 1971.
[15] T. K. Wu and L. L. Tsai, "Numerical analysis of electromagnetic fields in biological tissues," *IEEE Proc.*, vol. 62, pp. 1167–1168, Aug. 1974.
[16] T. K. Wu, "Electromagnetic scattering from arbitrarily-shaped lossy dielectric bodies," Ph.D. dissertation, University of Mississippi, University, 1976.
[17] Yu Chang and R. F. Harrington, "A surface formulation for characteristic modes of material bodies," Syracuse University, Electrical and Computer Engineering Dept. Tech. Report, No. 2, Contract N000A-67-A-0378-006, 1976.
[18] L. L. Tsai and T. K. Wu, "Scattering from lossy dielectric bodies of revolution," *1975 USNC/URSI Meeting Digest*, Boulder, CO, p. 128, Oct. 1975.
[19] J. R. Wait, *Electromagnetic Radiation from Cylindrical Structures*. New York: Pergamon Press, 1959.
[20] C. C. Johnson, C. H. Durney, and H. Massoudi, "Long-wavelength electromagnetic power absorption in prolate spheroidal models of man and animals," *IEEE Trans. Microwave Theory Tech.*, vol. MTT-23, pp. 739–747, Sept. 1975.

Field and Power Density Distributions of the Dipolar Modes in a Partially Filled Cylindrical Plasma Waveguide

GAR LAM YIP, SENIOR MEMBER, IEEE, AND SON LE-NGOC

***Abstract*—The field and power density distributions for the dipolar modes in a partially filled plasma waveguide have been studied at operating points in the vicinity of the plasma, the surface wave, and the gyro**

Manuscript received June 30, 1975; revised April 30, 1976. This work was supported by the National Research Council of Canada.
G. L. Yip is with the Department of Electrical Engineering, McGill University, Montreal, P.Q., Canada.
S. Le-Ngoc was with the Department of Electrical Engineering, McGill University, Montreal, P.Q., Canada. He is now with Pratt and Whitney Aircraft, Montreal, P.Q., Canada.